



Dynamical topology in ferroelectric nanostructures by $\frac{1}{2}[1\bar{1}0](110)$ dislocations in SrTiO_3

Kairi Masuda ^{*}, Takahiro Shimada , and Takayuki Kitamura

Department of Mechanical Engineering and Science, Kyoto University, Nishikyo-ku, Kyoto 615-8540, Japan



(Received 1 December 2020; accepted 9 February 2021; published 24 February 2021)

Dynamical topology in ferroelectrics such as polarization rotation begins to attract interest because it brings new opportunities to generate properties that the static states cannot achieve. However, polarization behavior cannot be complicated under the spatially homogeneous electric fields that ferroelectrics are typically subjected to. Here, we demonstrate that a ferroelectric nanostructure with polarization rotation under cyclic electric fields is induced by a $\frac{1}{2}[1\bar{1}0](110)$ dislocation in SrTiO_3 . Phase-field simulations show that an elastic field specific to the dislocation causes an L-shaped ferroelectric nanoregion in paraelectric SrTiO_3 while a trajectory of polarization exhibits clockwise rotation under one cyclic electric field. Furthermore, we demonstrate that the trajectory exhibits a clockwise-oscillation-anticlockwise transition, depending on the angle of the one cyclic electric field, which leads to functionalities such as binary addition. This work provides a strategy to engineer polarization dynamics and expands the knowledge of topology and the application of ferroelectrics.

DOI: [10.1103/PhysRevB.103.054114](https://doi.org/10.1103/PhysRevB.103.054114)

I. INTRODUCTION

Topological objects such as vortices, hedgehogs, and skyrmions formed by electric polarization in ferroelectrics are now a hot topic in materials science due to their exotic phenomena and potential applications [1–6]. The exploitation of such novel phases in ferroelectrics has mainly been conducted in static states, but dynamic states have begun to gain attention recently. According to the progress in the ability to manipulate materials in the time domain, dynamical equilibrium states, which are achieved by time-dependent but periodic external fields, provide new opportunities to generate properties that the static states cannot offer [7–9]. For example, lattice dynamics in $\text{YBa}_2\text{Cu}_3\text{O}_{6.5}$ during terahertz-frequency optical pulses are responsible for superconductivity up to room temperature [10]. In this context, it has been theoretically demonstrated that polarization rotation in ferroelectrics induces magnetization as a consequence of the Dzyaloshinskii-Moriya interaction, and a new concept of dynamical multiferroicity was proposed [11,12]. These studies indicate that dynamical topology, or characteristic trajectories of polarization behavior under electric fields, will result in unprecedented properties or functionalities. However, despite such growing interest, few such complicated polarization behaviors have been reported [13–16], and to the best of our knowledge, stand-alone ferroelectrics such as dots and rods with dynamical topology have never been reported although such low dimensionality is often required for device application [17]. The potential reason for this is that polarization is restricted by crystal orientations and cannot move freely. Moreover, the spatially homogeneous cyclic electric field that ferroelectrics are typically subjected to does not have chirality as an input, which is essential for topological configurations. Therefore, a novel mechanism is required that overcomes the restricted path and converts trivial inputs to topological outputs.

Dislocations, which are one-dimensional lattice defects in materials, are typically treated as the result of deformation and are not considered to be the origin of ferroelectricity. However, recent studies have shown that polarization is locally induced around dislocations in strontium titanate (SrTiO_3) due to strain concentration [18–20] although this material is ideally in the paraelectric state [21–24]. This induced ferroelectricity is an isolated ferroelectric nanostructure embedded within a paraelectric matrix [25]. Therefore, the properties of polarization can be engineered by unique strain distributions around dislocations, i.e., mechanical engineering by defects. So far, ferroelectricity around dislocations on the slip plane (010), which is parallel to the crystal orientation, has been mainly investigated. All polarization around these dislocations switches simultaneously as with typical ferroelectrics under spatially homogeneous electric fields because the strain region is formed only under the dislocation. However, since variations in slip planes disturb this monotonous region, ferroelectricity caused by other slip systems is expected to exhibit more complicated polarization dynamics.

Here, we demonstrate via phase-field simulations that an isolated ferroelectric nanostructure by an edge dislocation with the Burgers vector $\frac{1}{2}[1\bar{1}0]$ on the slip plane (110) ($\frac{1}{2}[1\bar{1}0](110)$ dislocation) in SrTiO_3 exhibits clockwise polarization rotation, i.e., dynamical topology under one cyclic electric field. Furthermore, we demonstrate that the dynamics exhibit a clockwise-oscillation-anticlockwise transition depending on the angle of the electric field, which leads to functionalities such as binary addition. These results provide a strategy to engineer polarization dynamics and expand our knowledge of topology and the application of ferroelectrics.

II. SIMULATION PROCEDURE

Figure 1 shows schematic images of this study. We focused on ferroelectricity and its dynamic behavior by the $\frac{1}{2}[1\bar{1}0](110)$ dislocation [26–28]. To this dislocation, we

^{*}masuda.kairi.64n@st.kyoto-u.ac.jp

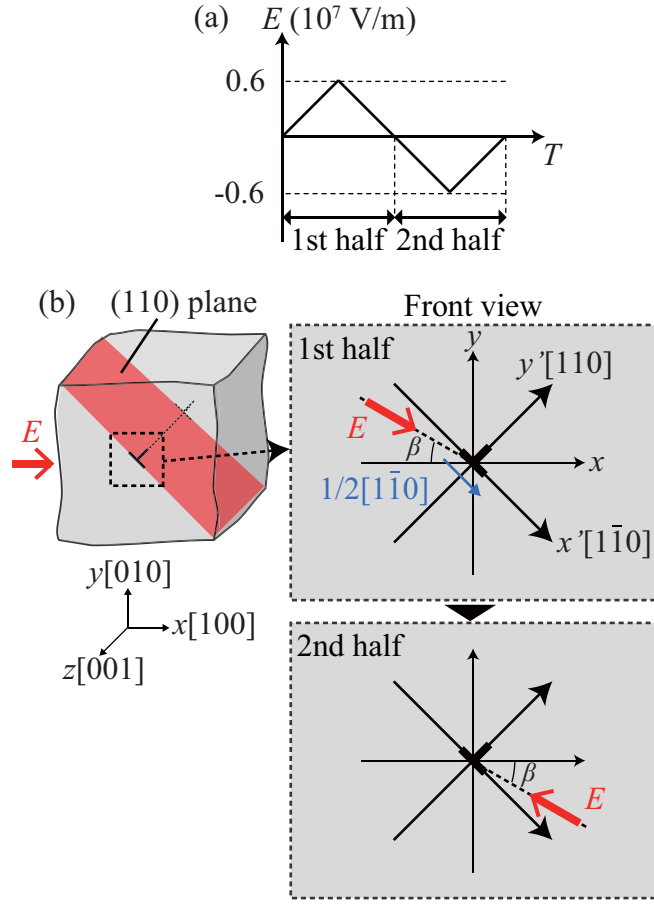


FIG. 1. Schematic illustrations of (a) one cyclic electric field E , where T is time and (b) a $\frac{1}{2}[1\bar{1}0](110)$ dislocation under the cyclic electric field from the x direction with an angle of β . The amplitude of the electric field is ± 0.6 (10^7 V/m) in this study. The blue arrow indicates the Burgers vector.

applied one cyclic electric field [Fig. 1(a)] from the x direction with an angle of β to evaluate the dynamical behavior. That is, the dislocation undergoes a spatially homogeneous electric field from the left in the first half of the cycle while it undergoes a spatially homogeneous electric field from the right in the second half at a fixed angle [Fig. 1(b)]. Note that such a cyclic electric field is the simplest field that ferroelectrics are subjected to. The formation of spontaneous polarization, $\mathbf{p} = (p_x, p_y, p_z)$, around the dislocation and its responses to the electric field at room temperature were carefully simulated by the phase-field modeling of SrTiO_3 based on the Ginzburg-Landau theory [29–32]. We employed a simulation model that consists of $128\Delta x \times 128\Delta x \times 1\Delta x$ grids with $\Delta x = 0.25$ nm, and the elastic field caused by the dislocation was introduced at the center as shown in Fig. S2 [33,34]. Although a periodic boundary condition was applied to the model, the dislocations are regarded as isolated because the distance between neighboring dislocations is 32 nm. Phase-field simulations were performed with the Fourier spectral iterative perturbation method [35–38] and the semi-implicit Fourier-spectral method [39,40] due to their computational efficiency. Full details of the computational details are available in the Supplemental Material [41].

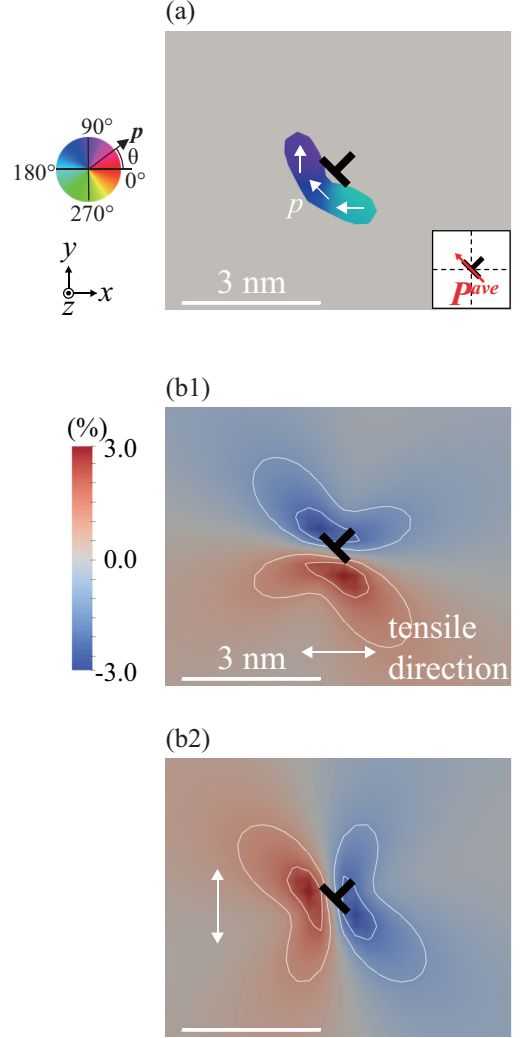


FIG. 2. (a) Polarization distribution, (b1) elastic strain distribution $\epsilon_{xx}^{\text{elas}}$, and (b2) $\epsilon_{yy}^{\text{elas}}$ around a $\frac{1}{2}[1\bar{1}0](110)$ dislocation in SrTiO_3 where the scale bars are 3 nm. In the polarization distribution, the contour region is where $|\mathbf{p}| > 0.08$ C/m² and its contour color and arrows indicate polarization directions. The inset is the averaged polarization direction. In the strain distributions, the contour indicates the magnitude of strain. The white lines indicate the contour lines of ± 1.0 and ± 2.0 (%), respectively.

III. RESULTS AND DISCUSSIONS

Figure 2(a) shows the polarization distribution around a $\frac{1}{2}[1\bar{1}0](110)$ dislocation. The contour region shows where ferroelectricity appears while the color shows the polarization directions. An L-shaped ferroelectric nanoregion is formed around the dislocation. In this region, polarization points in the x direction under the dislocation while it points in the y direction at the left side. The averaged polarization was calculated as according to

$$\mathbf{p}^{\text{ave}} = \frac{1}{V} \int_V \mathbf{p} dv, \quad (1)$$

where V is the volume of the ferroelectric nanoregion. Due to the L-shaped polarization structure, the averaged polarization points in the upper left direction as shown in the inset of

Fig. 2(a). To understand the appearance of ferroelectricity, the strain field around the $\frac{1}{2}110$ dislocation was investigated. The contour shows the magnitude of strain. The x -directional tensile strain is formed under the dislocation [Fig. 2(b1)] while tensile strain along the y direction is formed at the left side [Fig. 2(b2)]. Thus, an L-shaped tensile strain field is spontaneously formed around the $\frac{1}{2}[1\bar{1}0](110)$ dislocation. Since SrTiO₃ undergoes a paraelectric-ferroelectric phase transition by tensile strain [21–23], the L-shaped ferroelectric nanoregion is attributed to the L-shaped tensile strain field. This appearance of polarization may slightly relax the original elastic field of the dislocation because, at the tensile regions, strain levels before the polarization formation are slightly higher (Fig. S3). Note that a simpler dislocation, that is an edge dislocation with the Burgers vector $[100]$ on a slip plane (010) , does not exhibit such L-shaped ferroelectricity (Fig. S4) because the tensile region is formed only under the dislocation [18]. Therefore, this L-shaped polarization structure is specific to the $\frac{1}{2}[1\bar{1}0](110)$ dislocation.

Figure 3 shows the trajectories of the averaged polarization under one cyclic electric field. The trajectories move in the order of points a, b, c, d, e, f, g, h, and i, which correspond with the intensity of the cyclic electric field. When $\beta = 0^\circ$ [Fig. 3(a)], the averaged polarization points to the upper-left, the upper-right, the lower-right, the lower-left, and the upper-left direction in this order. That is, the polarization rotates clockwise under one cyclic electric field, which indicates that, despite the absence of chirality in the input, polarization dynamics exhibit topological behavior that typical ferroelectrics do not have. Noted that, in the case of a perfect crystal SrTiO₃, polarization does not exhibit such rotation by electric fields and the magnitude of polarization in this electric field range is much smaller than that around the dislocation (Fig. S5). These indicate that this polarization rotation can be attributed to ferroelectricity around the dislocation. Here, the ferroelectric nanoregion is a ferroelectric nanostructure embedded within a paraelectric matrix. Thus, an isolated ferroelectric nanostructure with dynamical topology can be tailored by a $\frac{1}{2}[1\bar{1}0](110)$ dislocation. This rotation shrinks with an increase of β [Fig. 3(b)] and, when $\beta = 45^\circ$ [Fig. 3(c)], the trajectory of polarization returns to the first position through the same path, i.e., oscillation, which indicates that the polarization dynamics are no longer topological. However, with a further increase of β , the polarization begins to rotate again but the direction is anticlockwise [Fig. 3(e)]. Therefore, the polarization dynamics undergo a clockwise-oscillation-anticlockwise transition depending on the angle of one cyclic electric field.

To elucidate the underlying mechanism of the polarization rotation, polarization distributions under one cyclic electric field with an angle of $\beta = 0^\circ$ were analyzed [Fig. 4]. Here, each distribution corresponds to the points in Fig. 3(a). At first, the averaged polarization points in the upper-left direction [Fig. 4(a)]. This state undergoes a spatially homogeneous electric field from the left. With an increase of the electric field, the ferroelectric nanoregion under the dislocation, which has polarization antiparallel to the field, preferentially shrinks [Fig. 4(b)]. As a result, polarization under the dislocation switches at point c of $E = 0.5$ (10^7 V/m), and the tail-to-tail configuration is formed [Fig. 4(c)]. At this point, the

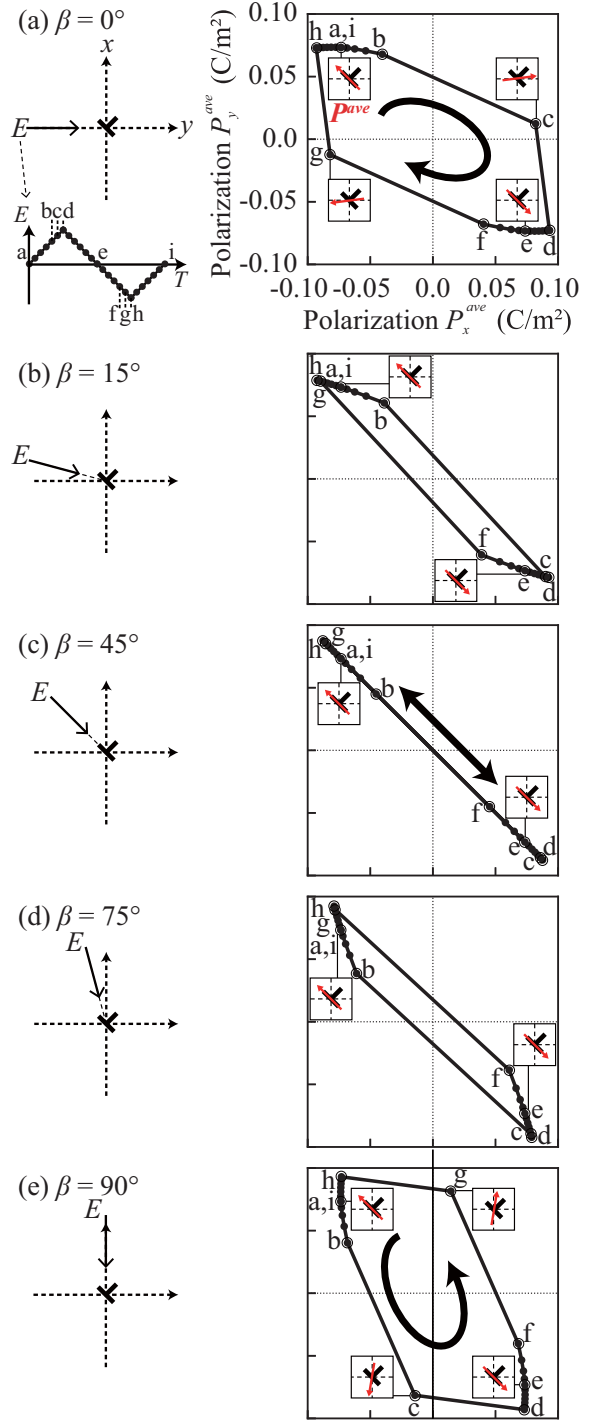


FIG. 3. Trajectories of averaged polarization \mathbf{P}^{ave} , under one cyclic electric field. Points a = 0.0, b = 0.4, c = 0.5, d = 0.6, e = 0.0, f = -0.4, g = -0.5, h = -0.6, and i = 0.0 (10^7 V/m), respectively. The insets show schematic illustrations of the averaged polarization directions at the corresponding points.

averaged polarization points in the upper-right direction. On the other hand, polarization at the left side of dislocation switches at point d of $E = 0.6$ (10^7 V/m), which results in the averaged polarization pointing in the lower-right direction

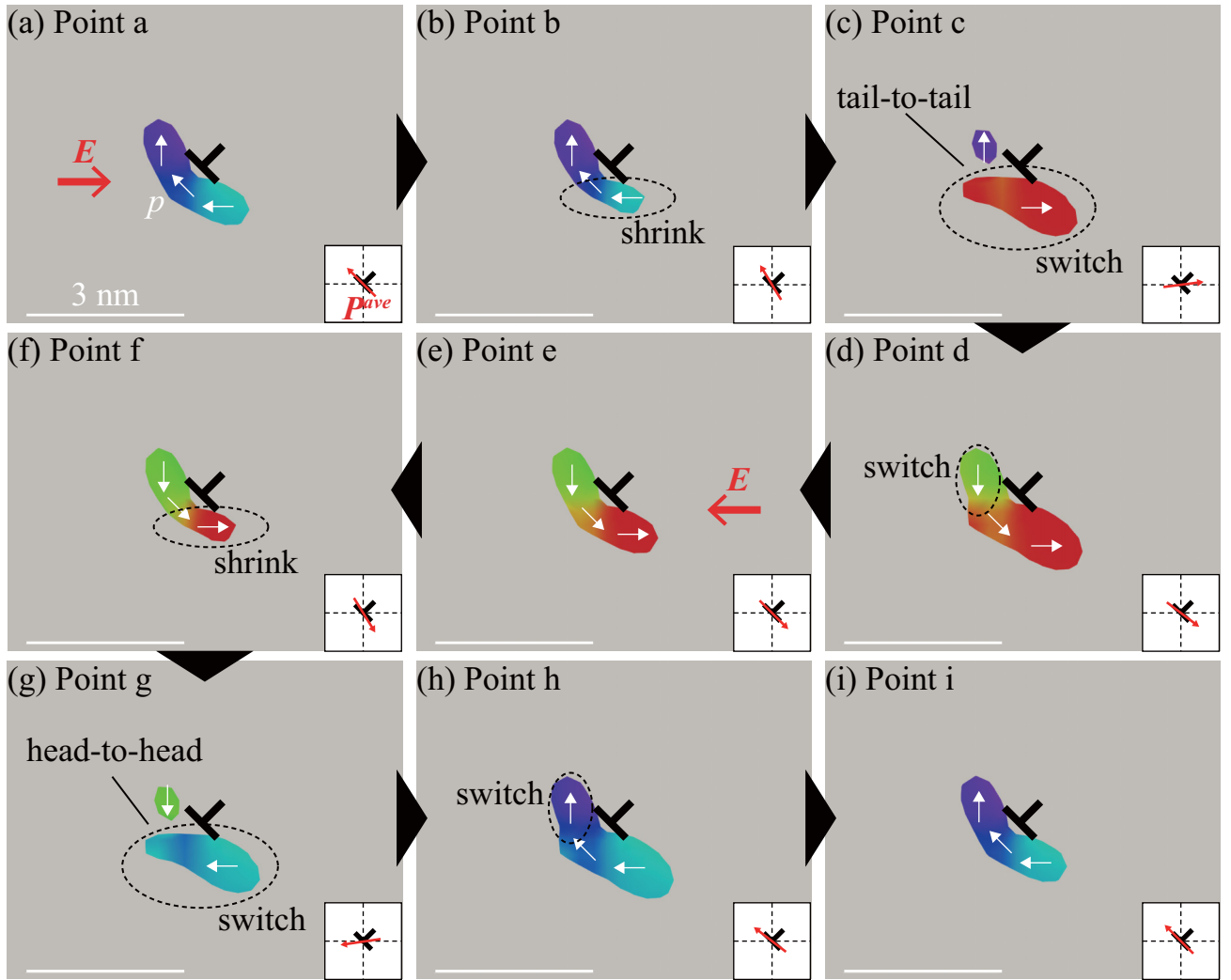


FIG. 4. Polarization distributions under one cyclic electric field with an angle of $\beta = 0^\circ$. The points correspond to those in Fig. 3(a). Here, polarization undergoes an electric field from the left in the first half of one cycle (points a–e) while it undergoes an electric field from the right in the second half (points e–i). White arrows indicate the directions of local polarization in the ferroelectric nanoregion while red arrows in the insets indicate the averaged polarization directions. The definition of the contour region is the same as in Fig. 2(a).

[Fig. 4(d)]. This unusual switching of polarization perpendicular to the field is attributed to the energetic instability of the tail-to-tail configuration due to the electrostatic interaction. With a decrease of the electric field, polarization is completely switched from the initial state at point e of $E = 0.0$ (10^7 V/m) [Fig. 4(e)]. Next, this state is subjected to the electric field from the right. With an increase of the electric field, the ferroelectric nanoregion under the dislocation preferentially shrinks and switches [Figs. 4(f) and 4(g)], the same as points b and c. However, at point g of $E = -0.5$ (10^7 V/m), the head-to-head configuration is formed, which is different from point c, and the averaged polarization points in the lower-left direction [Fig. 4(g)]. At point h of $E = -0.6$ (10^7 V/m), polarization at the left side of the dislocation switches to avoid the energetically unstable head-to-head configuration, and the averaged polarization points in the upper-left direction [Fig. 4(h)]. With a decrease of the electric field, the polarization configuration returns to the initial state at point i of $E = 0.0$ (10^7 V/m) as shown in Fig. 4(i).

Therefore, the switching path differs between going (points a–e) and returning (points e–i) despite the spatially homogeneous electric field due to the preferential polarization switching under the dislocation. This is the reason for the polarization rotation of Fig. 3(a), which is a different mechanism from those observed in ferroelectrics with intermediate monoclinic phases [13–15] and nanoporous PbTiO_3 [16]. On the other hand, the transition from the clockwise rotation to oscillation can be attributed to the fact that polarization at the left side of and under the dislocation is likely to switch at the same time by an increase of β . The transition from the oscillation to the anticlockwise rotation by a further increase of β could be due to preferential polarization switching at the left side of the dislocation. It should be noted that such a variety of switching behaviors, thus polarization trajectories, are not observed in a simpler dislocation, indicating that the above behaviors are unique to a $\frac{1}{2}[1\bar{1}0](110)$ dislocation (Figs. S6 and S7).

We investigated functionalities by the dynamical topology in a finite dimension in this study. As mentioned above, the

TABLE I. Polarization dynamics around a $\frac{1}{2}[1\bar{1}0](110)$ dislocation under one cyclic electric field. Symbols \circ and \times in the input column indicate applying/not applying electric fields and those in the output column indicate exhibiting/not exhibiting the motions.

	Input		Output	
	E_{0°	E_{90°	Oscillation	Rotation
No electric fields	\times	\times	\times	\times
$\beta = 0^\circ$	\circ	\times	\times	\circ
$\beta = 90^\circ$	\times	\circ	\times	\circ
$\beta = 45^\circ$	\circ	\circ	\circ	\times

polarization switching path exhibits rotation at $\beta = 0^\circ$ and 90° or oscillation at $\beta = 45^\circ$, as summarized in Table I. Here, we considered that an electric field with $\beta = 45^\circ$ is a superposition of those with $\beta = 0^\circ$ and 90° . Table I corresponds with the binary addition: $0 + 0 = 00$, $1 + 0 = 01$, $0 + 1 = 01$, $1 + 1 = 10$, which indicates arithmetic by polarization dynamics. Thus, an isolated or stand-alone ferroelectric nanostructure by a $\frac{1}{2}[1\bar{1}0](110)$ dislocation functions as a nano-half adder, which can be an alternative to conventional transistor-based circuits that have faced critical problems through miniaturization [42–45]. Furthermore, according to Juraschek *et al.*, polarization rotation is expected to induce magnetism [11], which suggests the ferroelectric nanostructure in this study may be a dynamical multiferroic nanoelement. Moreover, a recent proposal of an atom or spin heat engine [46,47] inspired us to see the result in terms of machinery. That is, a ferroelectric nanostructure in which polarization rotation is induced by an oscillation of an electric field can be regarded as a nanocrank mechanism, i.e., a building block of a nanomachine. These functionalities are completely different from those of the static counterpart, i.e., polarization vortices in nanodots.

Thus, an elastic field of $\frac{1}{2}[1\bar{1}0](110)$ dislocations induces an isolated ferroelectric nanostructure with unconventional dynamics, which is a new way to design topology and functionality in ferroelectrics. Although we have considered an isolated dislocation, the elastic field could be more complicated through effects from other dislocations or defects. This suggests that polarization behavior exhibits more diverse dynamical topologies such as eight-shaped and trefoil trajectories. Moreover, polarization switching affected by other dislocations can be regarded as a many-body system through elastic fields and electrostatic interactions. Thus, chaos phases could occur or be tuned depending on the density of dislocations. Since dynamical topology leads to functionalities; such topological and chaos phases surely bring novel and unprecedented functionalities.

IV. CONCLUSION

We have demonstrated that a ferroelectric nanostructure with dynamical topology can be tailored by a $\frac{1}{2}[1\bar{1}0](110)$ dislocation in SrTiO_3 . Phase-field simulations revealed that an elastic field around the dislocation induces an L-shaped ferroelectric nanoregion. Application of one cyclic electric field to this region results in preferential switching of the polarization under the dislocation and then the polarization at the left side switches. This results in clockwise polarization rotation. Furthermore, we demonstrated that the polarization dynamics exhibit a clockwise-oscillation-anticlockwise transition depending on the angle of the electric field, which can lead to functionalities such as binary addition. The results presented here demonstrate the mechanical engineering of polarization dynamics by defects, which is expected to lead to unprecedented topology and functionalities in ferroelectrics.

ACKNOWLEDGMENT

This work was supported by JSPS KAKENHI Grants No. JP18H05241, No. JP18H03753, and No. JP18K18807.

- [1] I. I. Naumov, L. Bellaiche, and H. Fu, Unusual phase transitions in ferroelectric nanodisks and nanorods, *Nature (London)* **432**, 737 (2004).
- [2] Y. Nahas, S. Prokhorenko, L. Louis, Z. Gui, I. Kornev, and L. Bellaiche, Discovery of stable skyrmionic state in ferroelectric nanocomposites, *Nat. Commun.* **6**, 8542 (2015).
- [3] T. Shimada, L. V. Lich, K. Nagano, J. S. Wang, J. Wang, and T. Kitamura, Polar superhelices in ferroelectric chiral nanosprings, *Sci. Rep.* **6**, 35199 (2016).
- [4] L. Li, X. Cheng, J. R. Jokisaari, P. Gao, J. Britson, C. Adamo, C. Heikes, D. G. Schlom, L. Q. Chen, and X. Pan, Defect-Induced Hedgehog Polarization States in Multiferroics, *Phys. Rev. Lett.* **120**, 137602 (2018).
- [5] A. K. Yadav, C. T. Nelson, S. L. Hsu, Z. Hong, J. D. Clarkson, C. M. Schlepütz, A. R. Damodaran, P. Shafer, E. Arenholz, L. R. Dedon, D. Chen, A. Vishwanath, A. M. Minor, L. Q. Chen, J. F. Scott, L. W. Martin, and R. Ramesh, Observation of polar vortices in oxide superlattices, *Nature (London)* **530**, 198 (2016).
- [6] S. Das, Y. L. Tang, Z. Hong, M. A. P. Gonçalves, M. R. McCarter, C. Klewe, K. X. Nguyen, F. Gómez-Ortiz, P. Shafer, E. Arenholz, V. A. Stoica, S. L. Hsu, B. Wang, C. Ophus, J. F. Liu, C. T. Nelson, S. Saremi, B. Prasad, A. B. Mei, D. G. Schlom, J. Íñiguez, P. García-Fernández, D. A. Muller, L. Q. Chen, J. Junquera, L. W. Martin, and R. Ramesh, Observation of room-temperature polar skyrmions, *Nature (London)* **568**, 368 (2019).
- [7] X. Li, T. Qiu, J. Zhang, E. Baldini, J. Lu, A. M. Rappe, and K. A. Nelson, Terahertz field-induced ferroelectricity in quantum paraelectric SrTiO_3 , *Science* **364**, 1079 (2019).
- [8] P. Beaud, S. L. Johnson, E. Vorobeve, U. Staub, R. A. De Souza, C. J. Milne, Q. X. Jia, and G. Ingold, Ultrafast Structural Phase Transition Driven by Photoinduced Melting of Charge and Orbital Order, *Phys. Rev. Lett.* **103**, 155702 (2009).
- [9] M. Sato, S. Takayoshi, and T. Oka, Laser-Driven Multiferroics and Ultrafast Spin Current Generation, *Phys. Rev. Lett.* **117**, 147202 (2016).

- [10] R. Mankowsky, A. Subedi, M. Först, S. O. Mariager, M. Cholle, H. T. Lemke, J. S. Robinson, J. M. Glowinski, M. P. Minitti, A. Frano, M. Fechner, N. A. Spaldin, T. Loew, B. Keimer, A. Georges, and A. Cavalleri, Nonlinear lattice dynamics as a basis for enhanced superconductivity in $\text{YBa}_2\text{Cu}_3\text{O}_{6.5}$, *Nature (London)* **516**, 71 (2014).
- [11] D. M. Juraschek, M. Fechner, A. V. Balatsky, and N. A. Spaldin, Dynamical multiferroicity, *Phys. Rev. Materials* **1**, 014401 (2017).
- [12] K. Dunnett, J. X. Zhu, N. A. Spaldin, V. Juričić, and A. V. Balatsky, Dynamic Multiferroicity of a Ferroelectric Quantum Critical Point, *Phys. Rev. Lett.* **122**, 057208 (2019).
- [13] H. Fu and R. E. Cohen, Polarization rotation mechanism for ultrahigh electromechanical response in single-crystal piezoelectrics, *Nature (London)* **403**, 281 (2000).
- [14] J. Paul, T. Nishimatsu, Y. Kawazoe, and U. V. Waghmare, Polarization rotation, switching, and electric-field-temperature phase diagrams of ferroelectric BaTiO_3 : A molecular dynamics study, *Phys. Rev. B* **80**, 024107 (2009).
- [15] J. Sinsheimer, S. J. Callori, B. Bein, Y. Benkara, J. Daley, J. Coraor, D. Su, P. W. Stephens, and M. Dawber, Engineering Polarization Rotation in a Ferroelectric Superlattice, *Phys. Rev. Lett.* **109**, 167601 (2012).
- [16] L. V. Lich, T. Shimada, S. Sepideh, J. Wang, and T. Kitamura, Multilevel hysteresis loop engineered with ferroelectric nanometamaterials, *Acta Mater.* **125**, 202 (2017).
- [17] J. F. Scott, Applications of modern ferroelectrics, *Science* **315**, 954 (2007).
- [18] K. Masuda, L. V. Lich, T. Shimada, and T. Kitamura, Periodically-arrayed ferroelectric nanostructures induced by dislocation structures in strontium titanate, *Phys. Chem. Chem. Phys.* **21**, 22756 (2019).
- [19] P. Hirel, M. Mrovec, and C. Elsässer, Atomistic simulation study of $\langle 110 \rangle$ dislocations in strontium titanate, *Acta Mater.* **60**, 329 (2012).
- [20] P. Gao, S. Yang, R. Ishikawa, N. Li, B. Feng, A. Kumamoto, N. Shibata, P. Yu, and Y. Ikuhara, Atomic-Scale Measurement of Flexoelectric Polarization at SrTiO_3 Dislocations, *Phys. Rev. Lett.* **120**, 267601 (2018).
- [21] H. Uwe and T. Sakudo, Stress-induced ferroelectricity and soft phonon modes in SrTiO_3 , *Phys. Rev. B* **13**, 271 (1976).
- [22] J. H. Haeni, P. Irvin, W. Chang, R. Uecker, P. Reiche, Y. L. Li, S. Choudhury, W. Tian, M. E. Hawley, B. Craigo, A. K. Tagantsev, X. Q. Pan, S. K. Streiffer, L. Q. Chen, S. W. Kirchoefer, J. Levy, and D. G. Schlom, Room-temperature ferroelectricity in strained SrTiO_3 , *Nature (London)* **430**, 758 (2004).
- [23] A. Vasudevarao, A. Kumar, L. Tian, J. H. Haeni, Y. L. Li, C. J. Eklund, Q. X. Jia, R. Uecker, P. Reiche, K. M. Rabe, L. Q. Chen, D. G. Schlom, and V. Gopalan, Multiferroic Domain Dynamics in Strained Strontium Titanate, *Phys. Rev. Lett.* **97**, 257602 (2006).
- [24] G. Shirane and Y. Yamada, Lattice-dynamical study of the 110° K phase transition in SrTiO_3 , *Phys. Rev.* **177**, 858 (1969).
- [25] I. Sugiyama, N. Shibata, Z. Wang, S. Kobayashi, T. Yamamoto, and Y. Ikuhara, Ferromagnetic dislocations in antiferromagnetic NiO , *Nat. Nanotechnol.* **8**, 266 (2013).
- [26] T. Matsunaga and H. Saka, Transmission electron microscopy of dislocations in SrTiO_3 , *Philos. Mag. Lett.* **80**, 597 (2000).
- [27] K. Takehara, Y. Sato, T. Tohei, N. Shibata, and Y. Ikuhara, Titanium enrichment and strontium depletion near edge dislocation in strontium titanate $[001]/(110)$ low-angle tilt grain boundary, *J. Mater. Sci.* **49**, 3962 (2014).
- [28] P. Hirel, P. Carrez, and P. Cordier, From glissile to sessile: Effect of temperature on $\langle 110 \rangle$ dislocations in perovskite materials, *Scr. Mater.* **120**, 67 (2016).
- [29] G. Sheng, Y. L. Li, J. X. Zhang, S. Choudhury, Q. X. Jia, V. Gopalan, D. G. Schlom, Z. K. Liu, and L. Q. Chen, Phase transitions and domain stabilities in biaxially strained (001) SrTiO_3 epitaxial thin films, *J. Appl. Phys.* **108**, 084113 (2010).
- [30] G. Sheng, Y. L. Li, J. X. Zhang, S. Choudhury, Q. X. Jia, V. Gopalan, D. G. Schlom, Z. K. Liu, and L. Q. Chen, A modified Landau-Devonshire thermodynamic potential for strontium titanate, *Appl. Phys. Lett.* **96**, 232902 (2010).
- [31] Y. L. Li, S. Choudhury, J. H. Haeni, M. D. Biegalski, A. Vasudevarao, A. Sharan, H. Z. Ma, J. Levy, V. Gopalan, S. Trolrier-McKinstry, D. G. Schlom, Q. X. Jia, and L. Q. Chen, Phase transitions and domain structures in strained pseudocubic (100) SrTiO_3 thin films, *Phys. Rev. B* **73**, 184112 (2006).
- [32] B. K. Choudhury, K. V. Rao, and R. N. P. Choudhury, Dielectric properties of SrTiO_3 single crystals subjected to high electric fields and later irradiated with X-rays or γ -rays, *J. Mater. Sci.* **24**, 3469 (1989).
- [33] J. P. Hirth and J. Lothe, *Theory of Dislocations* (Krieger Publishing Company, Malabar, FL, 1982).
- [34] H. H. Wu, J. Wang, S. G. Cao, L. Q. Chen, and T. Y. Zhang, Micro-/macro-responses of a ferroelectric single crystal with domain pinning and depinning by dislocations, *J. Appl. Phys.* **114**, 164108 (2013).
- [35] J. J. Wang, X. Q. Ma, Q. Li, J. Britson, and L. Q. Chen, Phase transitions and domain structures of ferroelectric nanoparticles: Phase field model incorporating strong elastic and dielectric inhomogeneity, *Acta Mater.* **61**, 7591 (2013).
- [36] J. J. Wang, Y. Song, X. Q. Ma, L. Q. Chen, and C. W. Nan, Static magnetic solution in magnetic composites with arbitrary susceptibility inhomogeneity and anisotropy, *J. Appl. Phys.* **117**, 043907 (2015).
- [37] P. Yu, S. Y. Hu, L. Q. Chen, and Q. Du, An iterative-perturbation scheme for treating inhomogeneous elasticity in phase-field models, *J. Comput. Phys.* **208**, 34 (2005).
- [38] P. Song, T. Yang, Y. Ji, Z. Wang, Z. Yang, L. Q. Chen, and L. Chen, A comparison of Fourier spectral iterative perturbation method and finite element method in solving phase-field equilibrium equations, *Commun. Comput. Phys.* **21**, 1325 (2017).
- [39] L. Q. Chen and J. Shen, Applications of semi-implicit Fourier-spectral method to phase field equations, *Comput. Phys. Commun.* **108**, 147 (1998).
- [40] H. L. Hu and L. Q. Chen, Three-dimensional computer simulation of ferroelectric domain formation, *J. Am. Ceram. Soc.* **81**, 492 (1998).
- [41] See Supplemental Material at <http://link.aps.org/supplemental/10.1103/PhysRevB.103.054114> for computational details.
- [42] K. J. Kuhn, Considerations for ultimate CMOS scaling, *IEEE Trans. Electron Devices* **59**, 1813 (2012).
- [43] E. Pop, S. Sinha, and K. E. Goodson, Heat generation and transport in nanometer-scale transistors, *Proc. IEEE* **94**, 1587 (2006).

- [44] S. Manipatruni, D. E. Nikonov, and I. A. Young, Beyond CMOS computing with spin and polarization, *Nat. Phys.* **14**, 338 (2018).
- [45] S. Manipatruni, D. E. Nikonov, C. C. Lin, T. A. Gosavi, H. Liu, B. Prasad, Y. L. Huang, E. Bonturim, R. Ramesh, and I. A. Young, Scalable energy-efficient magnetoelectric spin-orbit logic, *Nature (London)* **565**, 35 (2019).
- [46] J. Roßnagel, S. T. Dawkins, K. N. Tolazzi, O. Abah, E. Lutz, F. Schmidt-Kaler, and K. Singer, A single-atom heat engine, *Science* **352**, 325 (2016).
- [47] D. von Lindenfels, O. Gräß, C. T. Schmiegelow, V. Kaushal, J. Schulz, M. T. Mitchison, J. Goold, F. Schmidt-Kaler, and U. G. Poschinger, Spin Heat Engine Coupled to a Harmonic-Oscillator Flywheel, *Phys. Rev. Lett.* **123**, 080602 (2019).